3-28-2006

Nanoindentation of Layered Materials with a Nonhomogeneous Interface

Praveen K. Chalasani
University of South Florida

Nanoindentation of Layered Materials with a Nonhomogeneous Interface

by

Praveen K. Chalasani

A thesis submitted in partial fulfillment
of the requirements for the degree of
Master of Science in Mechanical Engineering
Department of Mechanical Engineering
College of Engineering
University of South Florida

Major Professor: Autar K. Kaw, Ph.D.
Daniel Hess, Ph.D.
Ashok Kumar, Ph.D.

Date of Approval
March 28, 2006

Keywords: thin film, substrate, mechanical properties, shear stress, indenter

ACKNOWLEDGMENT

I express my sincere thanks to my major professor Autar K. Kaw who helped me at every step of my thesis and provided me with much needed financial support. He is always ready to help students in all situations.

I thank Dr. Ashok Kumar and Dr. Daniel Hess for their help as committee members. I want to thank my fellow graduate student Cuong Nguyen for helping me with the Design of Experiments. I thank Department of Mechanical Engineering for the financial support. I also thank Sue and other office staff for their support during the course of my study.

TABLE OF CONTENTS

LIST OF TABLES

LIST OF FIGURES

LIST OF NOMENCLATURE

$2a$ - Indentor width.

h_1 - Layer width.

h_2 - Interface width.

E_1 - Young's modulus of layer.

E_2 - Young's modulus of interface.

E_3 - Young's modulus of half-plane.

ν_1 - Poisson's ratio of layer.

ν_2 - Poisson's ratio of interface.

ν_3 - Poisson's ratio of half-plane.

u_1 - Displacement field along x-direction in layer.

u_2 - Displacement field along x-direction in interface.

u_3 - Displacement field along x-direction in half-plane.

υ_1 - Displacement field along y-direction in layer.

υ_2 - Displacement field along y-direction in interface.

υ_3 - Displacement field along y-direction in half-plane

σ_{xx} - Stress field along x-direction.

σ_{yy} - Stress field along *y*-direction.

σ_{xy} - Shear stress field.

μ_3 - Shear modulus for half-plane.

L - Applied Load.

p - Applied pressure distribution.

d - Contact depth

NANOINDENTATION OF LATERED MATERIALS WITH A NONHOMOGENEOUS INTERFACE

Praveen K. Chalasani

ABSTRACT

Indentation is used as a technique for mechanical characterization of materials for a long time. In the last few decades, new techniques of mechanical characterization at micro and nano level using indentation have been developed. Mechanical character-ization of thin films has become an important area of research because of their crucial role in modern technological applications.

Theoretical and computational models of indentation are less time consuming, cost effective, and flexible. Many researchers have investigated mechanical properties of thin films using theoretical and computational models.

In this study, an indentation model for a thin layer-substrate geometry with the possibility of nonhomogeneous or homogeneous interface of finite thickness between layer and substrate has been developed. The layer and substrate can be nonhomogeneous or homogeneous. Three types of indenters are modeled: 1) Uniform pressure indenter 2) Flat indenter 3) Smooth indenter. Contact depth, maximum interfacial normal stress and maximum interfacial shear stress play an important role in design and mechanical characterization of thin films using indentation and the effect of modeling the interface as homogeneous and nonhomogeneous on these parameters is studied.

A sensitivity analysis is also conducted to find the effect of indentation area, substrate to layer Young's modulus ratio, layer to interface thickness ratio on contact depth and critical interfacial stresses.

CHAPTER 1

INTRODUCTION

Thin film coatings play an important role in modern technological applications. Thin films of micro and nano thickness are not uncommon in modern technological applications. So, mechanical characterization of thin films has become an important area of research. During early 1980s, it was found that load sensing indentation can be used to obtain mechanical properties of thin films and surfaces. Instruments that can produce sub-micron level indentations were developed. Since then extensive research has been done on depth sensing indentation and analysis of experimental data to obtain mechanical properties of materials.

1.1 Literature survey

The procedure for depth sensing indentation is as follows. Load that varies linearly or in steps is applied to material while continuously measuring the indentation depth. Loading is followed by unloading and the data obtained is plotted to get load-displacement curve. Since it is time consuming and difficult to measure contact area of indentor by direct observation of hardness impressions, a simple and indirect method was developed by Oliver, Hutchings and Pethica (1986). Their method is based on load-displacement data and indenter area function (cross-sectional area of indenter as a

function of distance from its tip). The idea behind the method is that at peak load, the material conforms to the shape of indenter to some depth. If this depth can be known from load displacement data, then the projected area can be estimated from indenter shape function.

So, the estimation of contact depth of indenter in material at peak load became prime focus of early depth sensing indentation research. Oliver et al (1986) found that final depth is a better estimate for contact depth than the depth at maximum load.

Doerner and Nix (1986) observed that unloading curve is linear at peak load. They proposed a method of extrapolating the linear portion of unloading curve to zero load and using the extrapolated depth as contact depth. Experiments confirmed that extrapolated depth gives better estimation of contact depth when compared to either depth at peak load, h_{max} or final depth, h_f.

Oliver and Pharr (1992) showed that unloading curve is not linear for all materials even at initial stages and developed an analysis technique that accounts for the curvature in unloading data to estimate contact depth that accounts for the curvature of unloading curve. The analysis is based on analytical solutions to different indentor geometries. The technique provides a physically justifiable procedure for determining contact depth.

The above mentioned methods are being used by researchers to obtain mechanical properties from load-displacement data.

Many researchers have investigated the mechanical properties of nano range thin films using nanoindentation. Some developed theoretical and computational indentation models.

Chen, Lei Liu, and Wang (2004) investigated the effects of thickness and different film-substrate combinations. They used aluminum and tungsten films on glass and silicon substrates so that they can have a combination of soft films on hard substrates and hard films on soft substrates. They reported the effect of substrate on measured film properties. They found that for a soft film on a hard substrate hardness decreases at small indentation depth, then remains constant, and increases with increasing indentation depth. For a hard film on a soft substrate, hardness increases at small indentation depth, then remains constant, and decreases with increasing indentation depth.

Chudoba, Schwarzer and Ritcher (2000) studied elastic properties of thin films by indentation measurements with a spherical indenter. They used an analytical solution for the elastic deformation of substrate to simulate load-displacement data. From this solution they could determine Young's modulus of thin films independent of substrate effects. Linss, Schwarzer, et al (2004) investigated the mechanical properties of graded thin films with varying Young's modulus using theoretical modeling and nanoindentation. They showed that a graded coating can be distinguished from a homogeneous layer by elastic indentation using a variety of different spherical indentors. Chudoba et al (2004) derived the correct moduli at the lower and top most part of the graded coating using a mathematical model. Their theoretical values are in agreement with values obtained from experiments.

1.2 Our study

In this study we investigated the effect of nonhomogeneous interface between film and substrate and quantified the effect of various parameters like film thickness, type of indentor, elastic modulus ratio, and contact depth of indentor. For this purpose we have modeled a homogeneous or nonhomogeneous thin layer on a homogeneous half-plane (substrate) separated by a nonhomogeneous or homogeneous interface. We used three different type of indenter loads

The advantage with the above model is mathematical formulation required is simple and readily available. Models for stress and displacement fields for a nonhomogeneous finite strip with exponential variation in Young's modulus and Poisson's ratio is available in literature (Delale and Erdogan, 1988; Kaw et al., 1992). Models for stress and displacement fields for a homogeneous half-plane are also present in literature (Delale and Erdogan, 1988; Kaw et al., 1992). Using the above mentioned mathematical models, the film-substrate model can be solved numerically with a high degree of accuracy.

CHAPTER 2

FORMULATION

2.1 Geometry

The geometry of the problem is shown in Fig 1. The model consists of two nonhomogeneous layers of infinite length and finite width h_1 and h_2, respectively deposited on a homogeneous half-plane. Loads of different distributions are applied symmetrically about x-axis over a length of $2a$ on the top layer. Young's modulus and Poisson's ratio vary exponentially along the width of nonhomogeneous layers where as, they are constant in the homogeneous half-plane. This model can be solved mathematically for displacements and stresses.

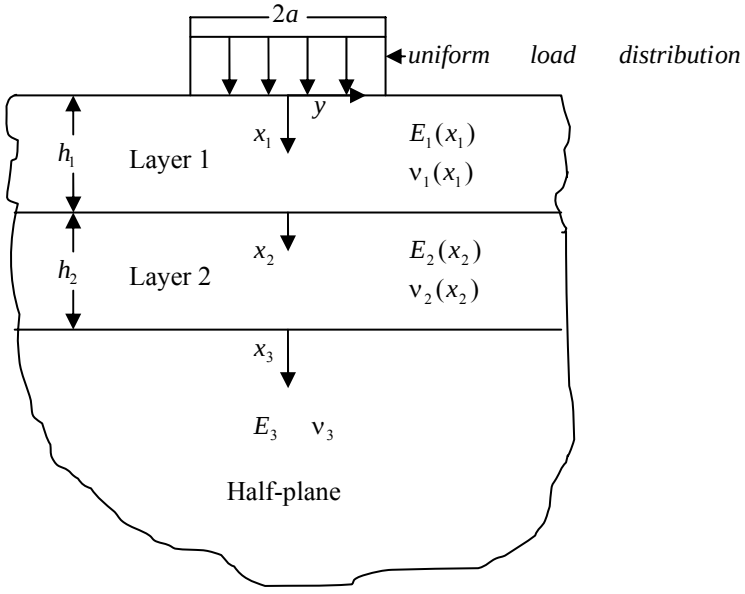

Figure 1: Schematic diagram of the layer-substrate model

2.2 Stress and displacement field equations

For i^{th} nonhomogeneous layer, Young's modulus, $E_i(x_i)$ and Poisson's ratio, $\nu_i(x_i)$ vary exponentially through the width as

$$E_i(x_i) = E_0^i e^{\beta_i x_i}, \tag{1}$$

$$\nu_i(x_i) = (a_0^i + b_0^i x_i) e^{\beta_i x_i}, \tag{2}$$

Where a_0^i, b_0^i, β_i and E_0^i are found using the Young's modulus and Poisson's ratios at the edges of the i^{th} strip $(x_i = 0, x_i = h_i)$.

The equations for stresses and displacement fields for i^{th} layer are given as (Delale and Erdogan, 1988; Kaw et al., 1992)

The displacement along the *x*-direction is given by

$$\begin{aligned} u_i(x_i, y) = \frac{2}{\pi E_0^i} \int_0^\infty \Bigg(& \frac{\eta^2}{2} \Bigg(\left[\frac{c_2^i(\eta) x_i}{m_2^i} + \frac{c_2^i(\eta)}{(m_2{}^i)^2} + \frac{c_1^i(\eta)}{m_2{}^i} \right] e^{-m_2^i x_i} \\ & + \left[\frac{c_4^i(\eta) x_i}{m_1{}^i} + \frac{c_4^i(\eta)}{(m_1{}^i)^2} + \frac{c_3^i(\eta)}{m_1{}^i} \right] e^{-m_1^i x_i} \Bigg) \\ & - \Big[b_0^i c_2^i(\eta) m_1^i x_i^2 + m_1^i x_i \left(a_0^i c_2^i(\eta) + b_0^i c_1^i(\eta) \right) \\ & + a_0^i c_1^i(\eta) m_1^i - b_0^i c_1^i(\eta) + a_0^i c_2^i(\eta) \Big] \frac{e^{m_1^i x_i}}{2} \\ & - \Big[b_0^i c_4^i(\eta) m_2^i x_i{}^2 + m_2^i x_i (a_0^i c_4^i(\eta) + b_0^i c_3^i(\eta)) \\ & + a_0^i c_3^i(\eta) m_2^i - b_0^i c_3^i(\eta) + a_0^i c_4^i(\eta) \Big] \frac{e^{m_2^i x_i}}{2} \Bigg) \cos(\eta y) d\eta, \end{aligned} \tag{3}$$

The displacement along *y*-direction is given by

$$\upsilon_i(x_i,y)=\frac{2}{\pi E_0^i}\int_0^\infty\left(\frac{1}{\eta}\Big[((m_1^i)^2(c_1^i(\eta)+c_2^i(\eta)x_i)\right.$$

$$+2m_1^ic_2^i(\eta))e^{-m_2^ix_i}+((m_2^i)^2(c_3^i(\eta)+c_4^i(\eta)x_i)$$

$$\left.+2m_2^ic_4^i(\eta)\right)e^{-m_1^ix_i}\ \Big]+\left(a_0^i+b_0^ix_i\right)\eta\Big[\ \left(c_1^i(\eta)+c_2^i(\eta)x_i\right)e^{m_1^ix_i}$$

$$\left.+(c_3^i(\eta)+c_4^i(\eta)x_i)e^{m_2^ix_i}\Big]\right)\frac{\sin(\eta y)}{2}d\eta\,, \tag{4}$$

The stress field is given by

$$\sigma_{xx}^i(x_i,y)=\frac{-2}{\pi}\int_0^\infty\frac{\eta^2}{2}\Big[\left(c_1^i(\eta)+c_2^i(\eta)x_i\right)e^{m_1^ix_i}+\left(c_3^i(\eta)+c_4^i(\eta)x_i\right)e^{m_2^ix_i}\Big]\cos(\eta y)d\eta\,, \tag{5}$$

$$\sigma_{yy}^i(x_i,y)=\frac{2}{\pi}\int_0^\infty\frac{1}{2}\Big(\Big[(m_1^i)^2\left(c_1^i(\eta)+c_2^i(\eta)x_i\right)+2m_1^ic_2^i(\eta)\Big]e^{m_1^ix_i}$$

$$+\Big[(m_2{}^i)^2\left(c_3{}^i(\eta)+c_4{}^i(\eta)x_i\right)+2m_2{}^ic_4^i(\eta)\Big]e^{m_2{}^ix_i}\Big)\cos(\eta y)d\eta\,, \tag{6}$$

$$\sigma_{xy}^i(x_i,y)=\frac{2}{\pi}\int_0^\infty\frac{\eta}{2}\Big(\Big[m_1{}^i\left(c_1{}^i(\eta)+c_2{}^i(\eta)x_i\right)+c_2^i(\eta)\Big]e^{m_1{}^ix_i}$$

$$+\Big[m_2^i\left(c_3^i(\eta)+c_4^i(\eta)x_i\right)+c_4^i(\eta)\Big]e^{m_2^ix_i}\Big)\sin(\eta y)d\eta\,. \tag{7}$$

where,

$$m_1^i=\frac{\beta_i}{2}-\left(\eta^2+\frac{\beta_i{}^2}{4}\right)^{\frac{1}{2}},\ \text{and} \tag{8}$$

and $$m_2^i=\frac{\beta_i}{2}+\left(\eta^2+\frac{\beta_i{}^2}{4}\right)^{\frac{1}{2}}. \tag{9}$$

The constants β_i, a_0^i and b_0^i in equations(1-9) are obtained from the Young's modulus and Poisson's ratio at the two edges $(x_i=0, x_i=h_i)$ of the i^{th} strip. The mathematical

equations for the constants when Young's modulus and Poisson's ratio are varying exponentially across the width are then given by

$$\beta_i = \frac{\ln\left(\frac{E_1^i}{E_0^i}\right)}{h_i}, \tag{10}$$

$$a_0^i = \nu_0^i, \tag{11}$$

$$b_0^i = \frac{\nu_1^i}{\left(h_i\left(e^{\beta_i h_i} - a_0^i\right)\right)}. \tag{12}$$

where

h_i = Width of i^{th} layer

E_0^i = Young's modulus of the i^{th} layer at $x_i = 0$

E_0^i = Young's modulus of the i^{th} layer at $x_i = h_i$

ν_0^i = Poisson's ratio of the i^{th} layer at $x_i = 0$,

ν_1^i = Poisson's ratio of the i^{th} layer at $x_i = h_i$.

The equations for stress and displacement fields for the homogeneous half plane are given by (Gupta, 1973)

The displacement in *y*-direction is given by

$$u_3(x_3, y) = \frac{2}{\pi}\int_0^\infty \left\{\frac{1}{\eta}\left[c_1^3 + \frac{\kappa_3 - 1}{2}c_2^3\right] + xc_2^3\right\} e^{-\eta x_3}\cos(\eta y)d\eta, \tag{13}$$

The displacement in *y*-direction is given by

$$\upsilon_3(x_3, y) = \frac{2}{\pi}\int_0^{\infty}\left\{\frac{1}{\eta}\left[c_1^3 - \frac{\kappa_3 + 1}{2}c_2^3\right] + xc_2^3\right\}e^{-\eta x_3}\sin(\eta y)d\eta, \tag{14}$$

The stress field is given by

$$\frac{\sigma_{xx}^3(x_3, y)}{2\mu_3} = -\frac{2}{\pi}\int_0^{\infty}\left[c_1^3 + \eta x_3 c_2^3\right]e^{-\eta x_3}\cos\eta y d\eta, \tag{15}$$

$$\frac{\sigma_{yy}^3(x_3, y)}{2\mu_3} = \frac{2}{\pi}\int_0^{\infty}\left[c_1^3 + (\eta x_3 - 2)c_2^3\right]e^{-\eta x_3}\cos\eta y d\eta \tag{16}$$

$$\frac{\sigma_{xy}^3(x_3, y)}{2\mu_3} = \frac{2}{\pi}\int_0^{\infty}\left[c_1^3 + (\eta x_3 - 1)c_2^3\right]e^{-\eta x_3}\sin\eta y d\eta \tag{17}$$

where κ_3 and shear modulus μ_3 are given by

$$\kappa_3 = 3 - 4\nu_3,$$

$$\mu_3 = \frac{E_3}{[2(1+\nu_3)]},$$

ν_3 = Poisson's ratio of half-plane,

E_3 = Young's modulus of half-plane.

2.3 Continuity conditions

When we use equations (3)-(8) to layer 1 and layer 2 ,we have eight unknown functions $c_1^1(\eta)$, $c_2^1(\eta)$, $c_3^1(\eta)$, $c_4^1(\eta)$, $c_1^2(\eta)$, $c_2^2(\eta)$, $c_3^2(\eta)$,and $c_4^2(\eta)$. From Equations (13)-(17) for half-plane we have two more unknown functions $c_1^3(\eta)$ and $c_2^3(\eta)$. To find stresses and displacements we need to solve for ten unknown functions present in the equations (3-8) and (13-17) ,using continuity and boundary conditions.

Continuity conditions are applied to stress and displacement equations (1-10) to get relationships between ten unknown functions $c_1^{\,1}(\eta)$, $c_2^1(\eta)$, $c_3^1(\eta)$, $c_4^1(\eta)$, $c_1^2(\eta)$, $c_2^2(\eta)$, $c_3^2(\eta)$, $c_4^2(\eta)$, $c_1^3(\eta)$ and $c_2^3(\eta)$.

The continuity conditions at the interface $(x_1 = h_1 \text{ or } x_2 = 0)$ of layer 1 and layer 2 are given by

$$\sigma_{xx}^1(h_1, y) = \sigma_{xx}^2(0, y), \tag{18}$$

$$\sigma_{xy}^1(h_1, y) = \sigma_{xy}^2(0, y), \tag{19}$$

$$u_1(h_1, y) = u_2(0, y), \tag{20}$$

$$\upsilon_1(h_1, y) = \upsilon_2(0, y). \tag{21}$$

The above continuity conditions provide four equations relating the variables. We get another four equations by applying continuity conditions at the interface between layer 2 and homogeneous half-plane, and are given by

$$\sigma_{xx}^2(h_2, y) = \sigma_{xx}^3(0, y), \tag{22}$$

$$\sigma_{xy}^2(h_2, y) = \sigma_{xy}^3(0, y), \tag{23}$$

$$u_2(h_2, y) = u_3(0, y), \tag{24}$$

$$\upsilon_2(h_2, y) = \upsilon_3(0, y). \tag{25}$$

Finally, we get two more equations relating unknown functions by applying boundary conditions to the stress and displacement field equations.

2.4 Boundary conditions

The boundary conditions on the top surface of the model are given by

$$\sigma_{xy}^{1}(0,y)=0 \tag{26}$$

$$\sigma_{xx}^{1}(0,y)=-p(y)\ ,\ \ -a\le y\le a$$

$$\sigma_{xx}^{1}(0,y)=0\ ,\ y>a\ . \tag{27}$$

where,

$p(y)$ is the applied pressure distribution,

$2a$ is the length over which the load is applied.

The two boundary conditions (26-27) along with eight continuity conditions (18-25) can be used to solve for ten unknown functions $c_1^{\,1}(\eta)$, $c_2^1(\eta)$, $c_3^1(\eta)$, $c_4^1(\eta)$, $c_1^2(\eta)$, $c_2^2(\eta)$, $c_3^2(\eta)$, $c_4^2(\eta)$, $c_1^3(\eta)$ and $c_2^3(\eta)$.

2.5 Types of loads

In this analysis we have used three different types of load distributions representing different types of indentors.

Flat Indentor:

The pressure distribution $p(y)$ for a flat indentor is given by

$$p(y) = \frac{L}{\pi\sqrt{a^2 - y^2}}, -a \le y \le a \tag{28}$$

where,

L = the applied load,

$2a$ = the loading length.

Smooth Indentor:

The pressure distribution $p(y)$ for a smooth indentor is given by

$$p(y) = \frac{2L}{\pi a^2}\sqrt{a^2 - y^2}, -a \le y \le a \tag{29}$$

where,

L is the applied load,

$2a$ is the loading length.

Uniform pressure:

The uniform pressure distribution is given by

$$p(y) = \frac{L}{2a}, -a \le y \le a \tag{30}$$

where,

L = the applied load,

$2a$ = the loading length.

2.6 Derivation of solution

The ten equations (18-27) resulting from continuity and boundary conditions can be arranged in the matrix form as

$$[A][B]=[C]$$

where,

$[A]$ is the coefficient matrix,

$[B]$ is the matrix of unknown functions,

$[C]$ is the right hand side array.

The above matrix form can be solved numerically for unknown functions. These functions are substituted in the stress and displacement field equations (3-8) and (13-17), and these equations are solved numerically to get stresses and displacements at any given point in the model.

CHAPTER 3

DESIGN OF EXPERIMENTS

3.1 Introduction

Design of experiments is a scientific way of planning the experiments involving more than one factor so that appropriate data that can be analyzed using statistical techniques is collected. Statistical analysis of collected data is important to reach valid conclusions. Since any valid scientific research involves experiments and statistical analysis of data collected from experiments, design of experiments involving multiple factors is an integral part of scientific study. In this chapter we discuss 2^k factorial design (Montgomery, 2001) which we used in our study.

3.2 Factorial designs

Factorial designs are used to study the combined effects of several factors on a response. Most experiments have two or more factors involved. Factorial designs are more useful for experiments involving more than two factors. There are several special cases of general factorial design that are used in research work because they form the basis for other designs of considerable practical importance. The most important special case of general factorial design is that of *k* factors, each at two different levels. This special case requires $2 \times 2 \times 2 \times ..... \times 2 = 2^k$ observations and is called 2^k factorial design.

3.3 2^k Factorial design

2^k Factorial design is a design with *k* factors each at two different levels. The model includes *k* main effects, $\binom{k}{2}$ two-factor interactions, $\binom{k}{3}$ three factor interactions, and one k-factor interaction. There are $2^k - 1$ total number of effects in a 2^k factorial design. For example, a 2^3 factorial design has $2^3 - 1$ total number of effects. In our study we have four important factors, so 2^4 factorial design is appropriate for our case. The following section discusses 2^4 factorial design in detail.

3.4 2^4 Factorial design

Let A, B, C, D are four main factors involved in the experiment. The total number of observations or runs required is given by $2^4 = 16$. Each factor has two different levels indicated by - and $+$. One level is indicated by - where as $+$ represents other level. There are $2^4 - 1$ total number of effects in factorial design, they are

Main effects: A, B, C, D

Two factor interactions: AB, AC, AD, BC, BD, and CD

Three factor interactions: ABC, ABD, ACD, and BCD

Four factor interaction: ABCD.

Table 1 shows the 16 runs or observations required for 2^4 design.

Table 1: Notations for experimental combinations

Run No	A	B	C	D	Run label	Response
1	-	-	-	-	(1)	Data1
2	+	-	-	-	a	Data2
3	-	+	-	-	b	Data3
4	+	+	-	-	ab	Data4
5	-	-	+	-	c	Data5
6	+	-	+	-	ac	Data6
7	-	+	+	-	bc	Data7
8	+	+	+	-	abc	Data8
9	-	-	-	+	d	Data9
10	+	-	-	+	ad	Data10
11	-	+	-	+	bd	Data11
12	+	+	-	+	abd	Data12
13	-	-	+	+	cd	Data13
14	+	-	+	+	acd	Data14
15	-	+	+	+	bcd	Data15
16	+	+	+	+	abcd	Data16

Table 2 below shows the contrast constants for the 2^4 design.

Table 2: Contrast constants for 2^4 design

Run label	A	B	AB	C	AC	BC	ABC	D	AD	BD	ABD	CD	ACD	BCD	ABCD
(1)	-	-	+	-	+	+	-	-	+	+	-	+	-	-	+
a	+	-	-	-	-	+	+	-	-	+	+	+	+	-	-
b	-	+	-	-	+	-	+	-	+	-	+	+	-	+	-
ab	+	+	+	-	-	-	-	-	-	-	-	+	+	+	+
c	-	-	+	+	-	-	+	-	+	+	-	-	+	+	-
ac	+	-	-	+	+	-	-	-	-	+	+	-	-	+	+

Table 2: Continued

bc	-	+	-	+	-	+	-	-	+	-	+	-	+	-	+
abc	+	+	+	+	+	+	+	-	-	-	-	-	-	-	-
d	-	-	+	-	+	+	-	+	-	-	+	-	+	+	-
ad	+	-	-	-	-	+	+	+	+	-	-	-	-	+	+
bd	-	+	-	-	+	-	+	+	-	+	-	-	+	-	+
abd	+	+	+	-	-	-	-	+	+	+	+	-	-	-	-
cd	-	-	+	+	-	-	+	+	-	-	+	+	-	-	+
acd	+	-	-	+	+	-	-	+	+	-	-	+	+	-	-
bcd	-	+	-	+	-	+	-	+	-	+	-	+	-	+	-
abcd	+	+	+	+	+	+	+	+	+	+	+	+	+	+	+

The contrast constants for interaction effects shown are obtained by multiplying the contrast constants of individual effects. For example, the contrast constant for interaction effect BC for run (1) is + because both B and C has - contrast constant for run (1).

Contrast:

The next step is to find contrasts from contrast constants. Contrast for each effect is obtained by multiplying the contrast column of each effect with the response column in Table 1 and then taking the sum of the elements of the resulting column. For example, for factor A contrast is obtained by multiplying column A in Table 2 with response column in Table 2 and adding all the elements of resulting column. So contrast for A is given by

Contrast A = (-Data1+Data2-Data3+Data4-Data5+Data6-Data7+Data8-
Data9+Data10-Data11+Data12-Data13+Data14-Data15+Data16)

Similarly we can find Contrasts for all the $2^4 - 1$ effects.

Sum of squares: The sum of squares for the effects are calculated using the following formulae.

$$SS = \frac{(Contrast)^2}{2^4 n}$$

where,

n = number of runs.

Total sum of squares: The total sum of squares is obtained by adding the individual sum of squares of effects.

$$SS_T = SS_A + SS_B + SS_C + ... + SS_{ABCD}$$

The percentage contribution of each of the effects is obtained by taking the ratio of sum of squares of effect to total sum of squares and then multiplying the result with 100. For example, the percentage contribution of effect A is given by

$$\text{Percentage contribution of A} = \frac{SS_A}{SS_T} \times 100 .$$

The factor having the highest percentage contribution is said to have the most effect on the experiment.

CHAPTER 4

RESULTS

4.1 Introduction

In this chapter we present the results obtained from FORTRAN program and statistical analysis. The layer-substrate indentation model discussed in chapter 2 can be solved mathematically for stresses and displacements using the formulation described in chapter 2. Our objective is to study the effect of nonhomogeneous interface between homogeneous layer and homogeneous substrate on contact depth at the surface, maximum normal stress and maximum shear stress at the interface and to quantify the effect of various parameters on the results using statistical analysis.

To achieve the above purpose we have used the formulation presented in chapter 2. Layer 1 in the model described in chapter 2 is our homogeneous layer and Layer 2 can be used as either nonhomogeneous or homogeneous interface between homogeneous layer and homogeneous substrate represented by homogeneous half-plane.

4.2 Contact depth

Contact depth, d is the depth through which the indentor is in contact with the material. It is obtained from the model by taking the difference of displacements at $x = 0$ at $y = 0$ and $y = a$.

$$d = u(0,a) - u(0,0)$$

We have obtained results for contact depth d for both homogeneous and nonhomogenous interface for all the three types of indentors, for different Young's modulus ratio and for different indentor width-layer thickness $\left(\frac{a}{h_1}\right)$ ratio. Below are the values we have chosen for each parameter.

Young's modulus ratio, $\frac{E_1}{E_3} : \frac{15}{200}, \frac{15}{120}, \frac{15}{60}, 1, \frac{60}{15}, \frac{120}{15}, \frac{200}{15}$

Indentor width-layer thickness ratio $\frac{a}{h_1} : \frac{1}{6}, \frac{1}{3}, \frac{1}{2}$

We had to choose Young's modulus ratio between $\frac{15}{200}$ and $\frac{200}{15}$ to keep the exponentially varying Poisson's ratio below 0.5.

Fig 2, Fig 4, and Fig 6 show how normalized vertical displacement difference $\frac{u(y) - u(0)\left(\pi a^2 E_1\right)}{\left(h_1 L\right)}$, varies with distance from indentor axis along surface for uniform indentor, flat indentor and spherical indentor, respectively. The figures contain plots for both nonhomogeneous and homogeneous interface.

Fig 3, Fig 5, and Fig 7 below are contact depth ratio $\frac{d_{nh}}{d_h}$ as a function of Young's modulus ratio plots for uniform indentor, flat indentor, and spherical indentor, respectively.

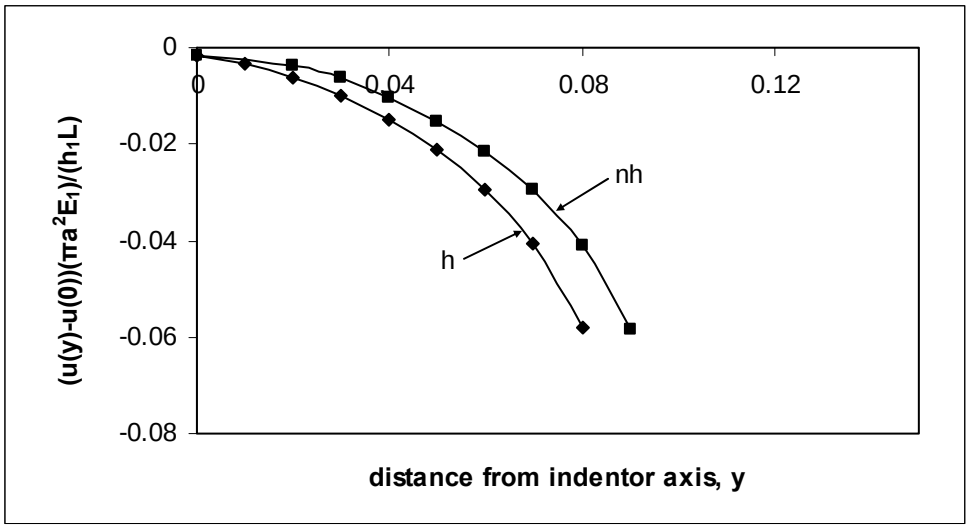

Figure 2: Normalized vertical displacement difference $(u(y)-u(0))(\pi a^2 E_1)/(h_1 L)$ as a function of distance along top surface from indentor axis for uniform pressure

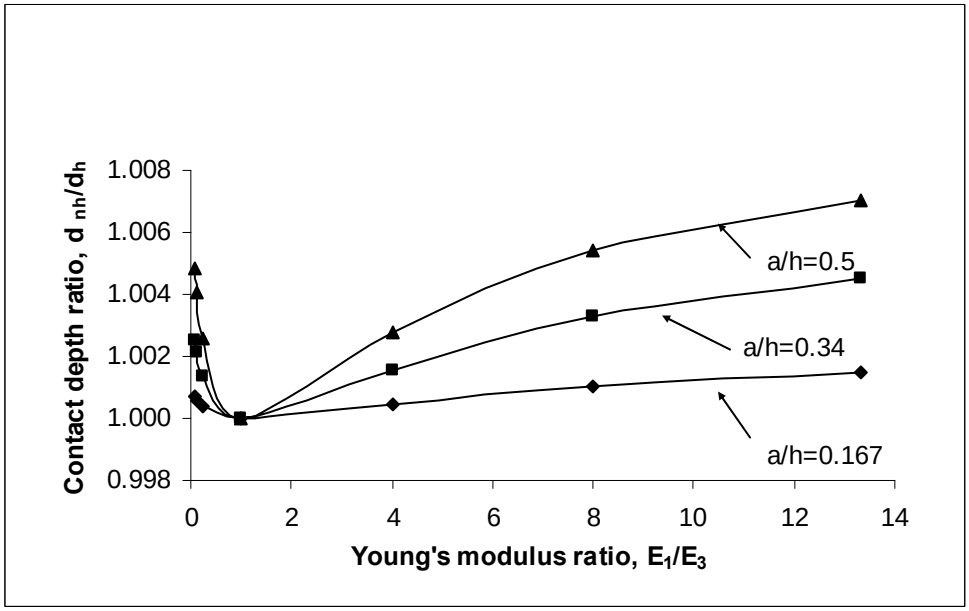

Figure 3: Contact depth ratio as a function of Young's modulus ratio between layer and substrate for uniform pressure

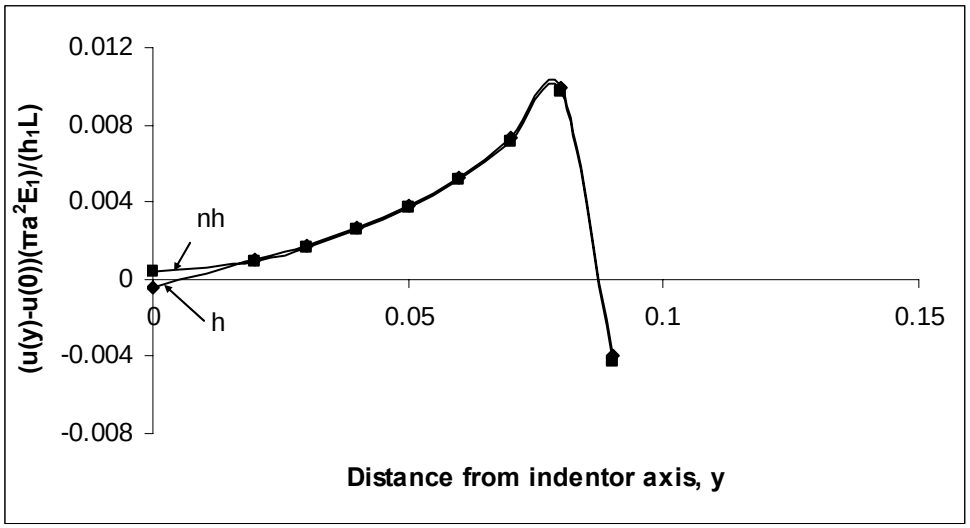

Figure 4: Normalized vertical displacement difference, $(u(y)-u(0))(\pi a^2 E_1)/(h_1 L)$ as a function of distance along top surface from indentor axis for flat indentor

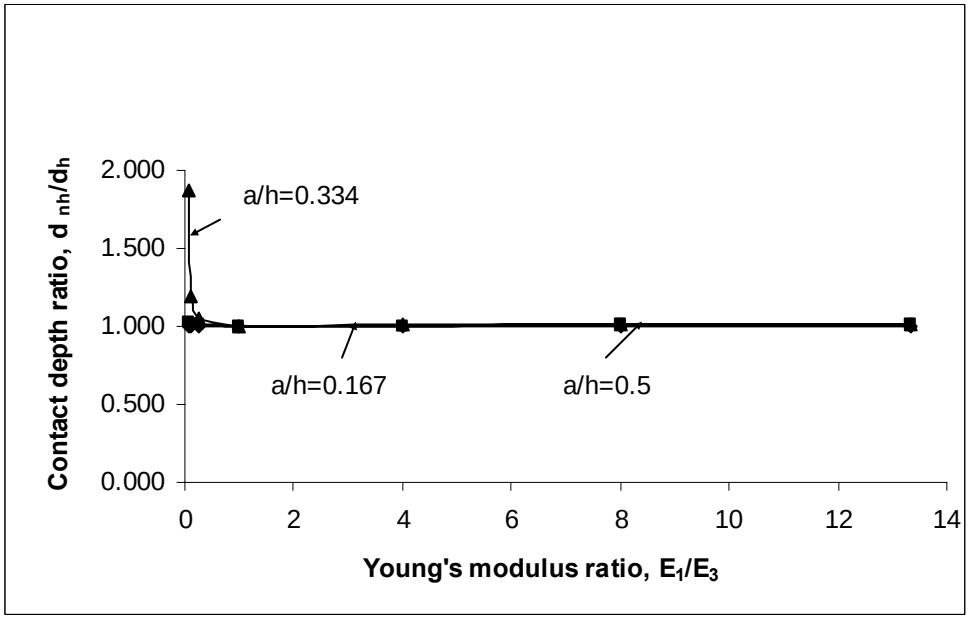

Figure 5: Contact depth ratio as a function of Young's modulus ratio between layer and substrate for flat indentor

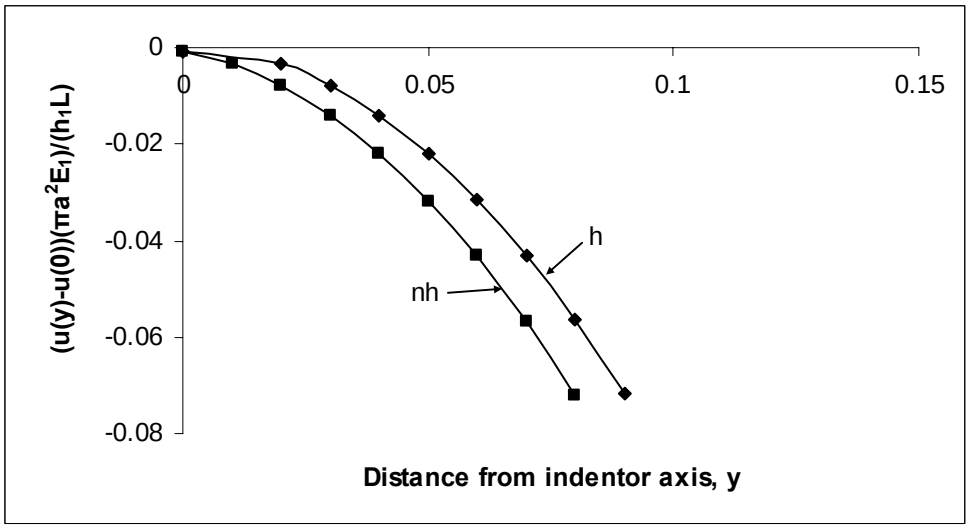

Figure 6: Normalized vertical displacement difference $(u(y)-u(0))(\pi a^2 E_1)/(h_1 L)$, as a function of distance along top surface from indentor axis for spherical indentor

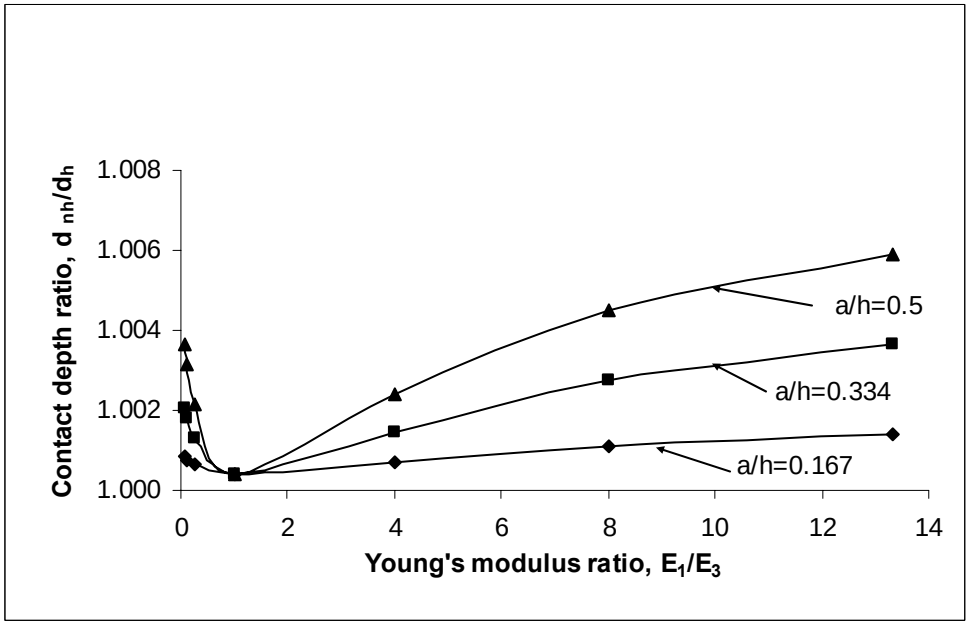

Figure 7: Contact depth ratio as a function of Young's modulus ratio between layer and substrate for spherical indentor

We can see from Fig 3, Fig 5, and Fig 7 the contact depth ratio $\frac{d_{non}}{d_{\hom}}$ is close to1.0 except for flat indentor where the ratio is close to 2.0 for values of $\frac{E_1}{E_3}$ close to zero and the ratio increases with increase in $\frac{a}{h_1}$ ratio. So there is no significant difference between contact depth values for homogeneous and nonhomogeneous interface either for soft layer on hard substrate, $\frac{E_1}{E_3} < 1.0$ or for hard layer on soft substrate, $\frac{E_1}{E_3} > 1.0$.

Also, from Fig 2, Fig 4 and Fig 6 one can notice that contact depth curves for homogeneous and nonhomogeneous interface are overlapping each other. So, we can conclude that for $0 < \frac{E_1}{E_3} < 13.33$, contact depth results are not effected by nonhomogeneous nature of interface.

4.3 Normal stress

The maximum normal stress $\sigma_{xx}\big|_{\max}$ at the interface should be maintained below a critical value to avoid debonding between layer and substrate. We have obtained results for maximum normal stress at the layer-substrate interface $\sigma_{xx}\big|_{\max}$ for both homogeneous and nonhomogenous interface for all the three types of indentors, for different Young's modulus ratio and for different $\frac{a}{h_1}$ ratio. Below are the values we have chosen for each parameter.

Young's modulus ratio, $\frac{E_1}{E_3} : \frac{15}{200}, \frac{15}{120}, \frac{15}{60}, 1, \frac{60}{15}, \frac{120}{15}, \frac{200}{15}$

Indentor width-layer thickness ratio, $\frac{a}{h_1} : \frac{1}{6}, \frac{1}{3}, \frac{1}{2}$

Fig 8, Fig 10, and Fig 12 show how normalized interface normal stress , $\sigma_{xx}(\pi a^2)/L$ changes with distance from indentor axis along interface for uniform pressure, flat indentor, and spherical indentor, respectively. The curves represent normal stress as a function of distance for homogeneous and nonhomogeneous interface.

Fig 9, Fig 11, and Fig 13 below are plots for maximum normal stress ratio as a function of Young's modulus ratio for uniform indentor, flat indentor, and spherical indentor respectively. The three different curves represent three different ratios between indentor width and layer thickness.

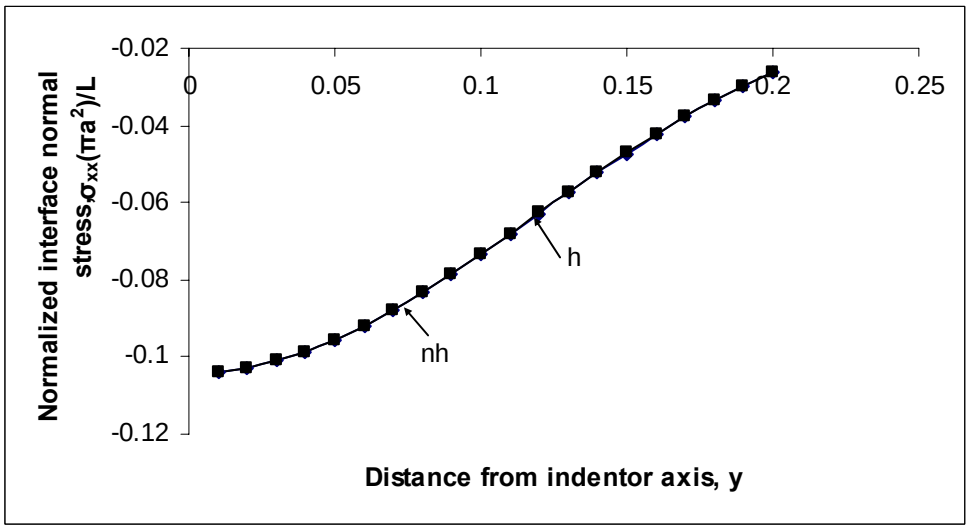

Figure 8: Normalized interface normal stress, $\sigma_{xx}(\pi a^2)/L$ at the layer-substrate interface as a function of distance along interface from indentor axis for uniform pressure

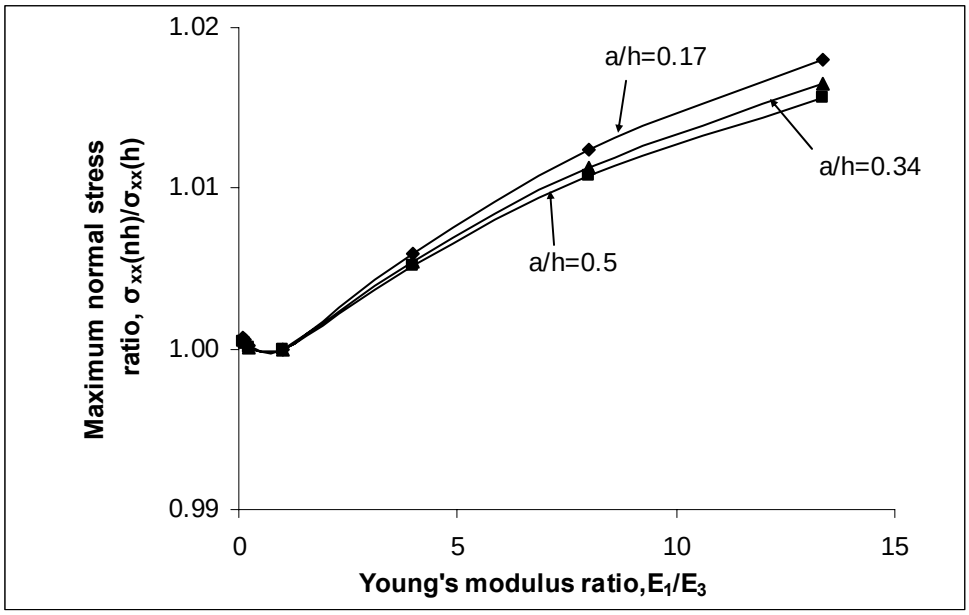

Figure 9: Maximum normal stress ratio along interface as a function of Young's modulus between layer and substrate for uniform pressure

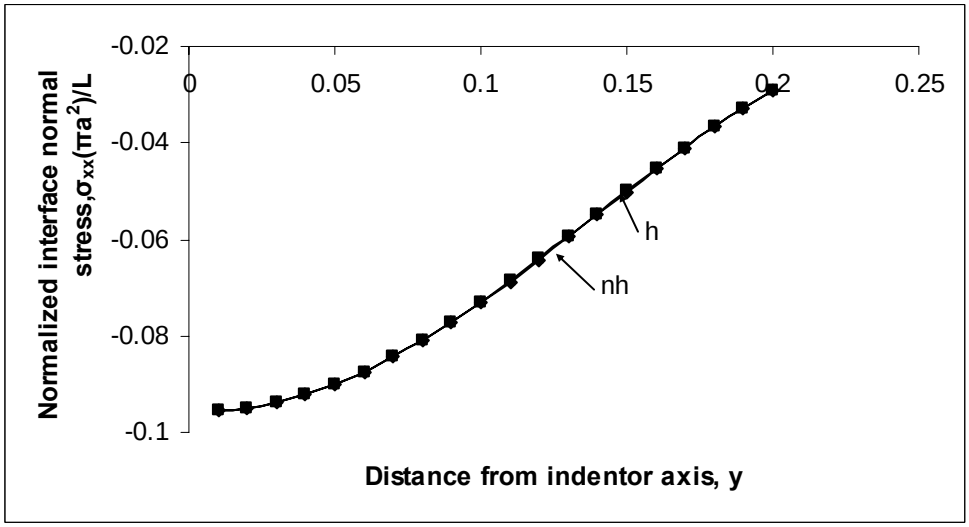

Figure 10: Normalized interface peel stress, $\sigma_{xx}(\pi a^2)/L$ at the layer-substrate interface as a function of distance along interface from indentor axis for flat indentor

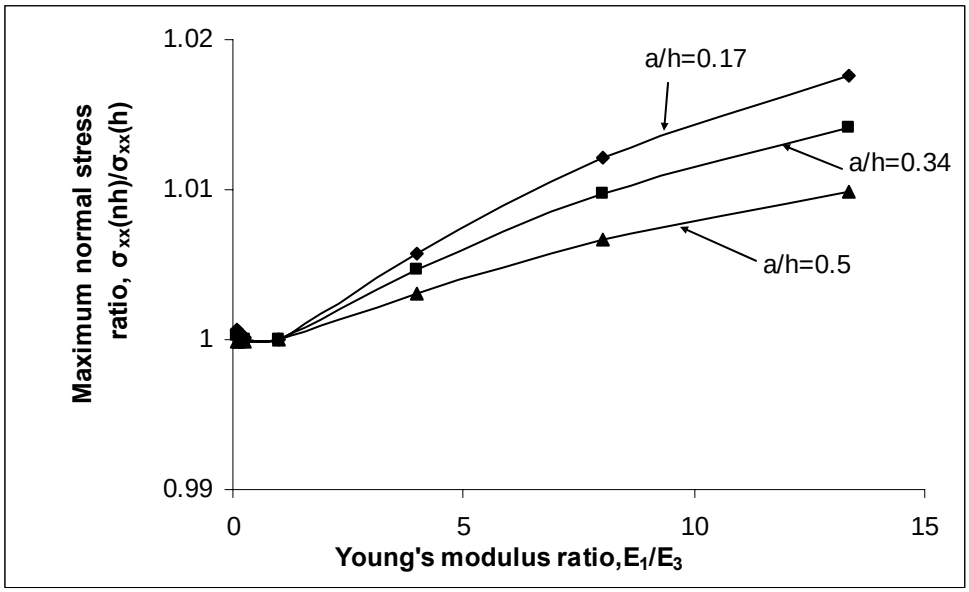

Figure 11: Maximum normal stress ratio along interface as a function of Young's modulus between layer and substrate for flat indentor

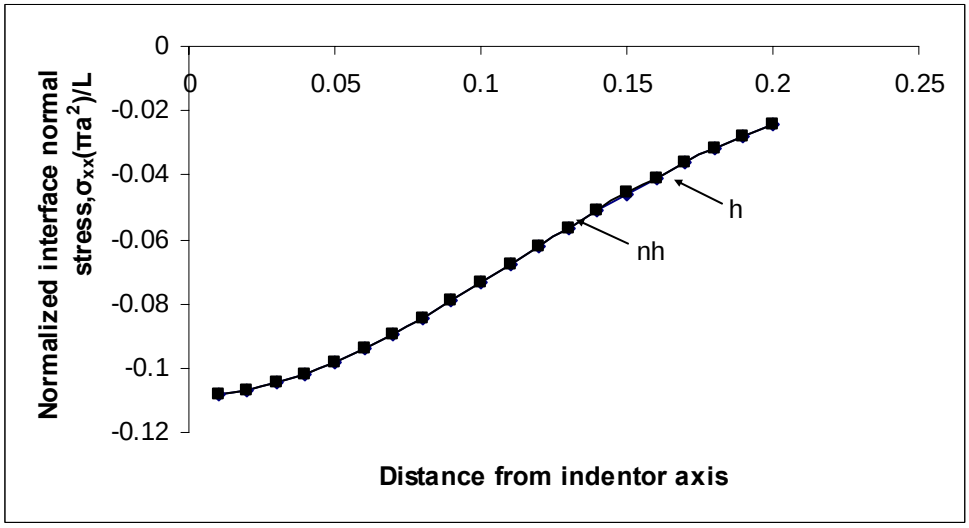

Figure 12: Normalized interface peel stress, $\sigma_{xx}(\pi a^2)/L$ at the layer-substrate interface as a function of distance along interface from indentor axis for spherical indentor

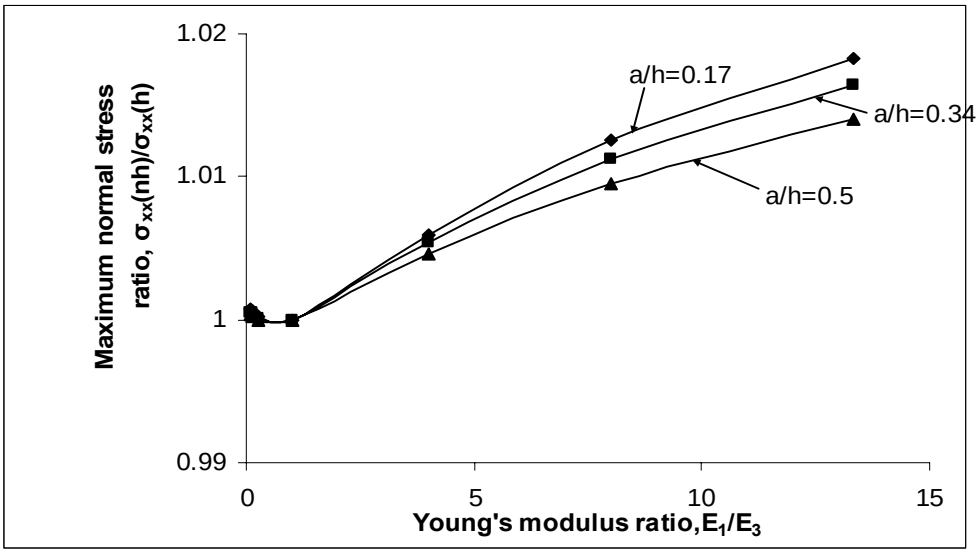

Figure 13: Maximum normal stress ratio along interface as a function of Young's modulus between layer and substrate for spherical indentor

W e can see from the above plots the maximum normal stress ratio $\frac{\sigma_{xx}(nh)}{\sigma_{xx}(h)}$ is close to 1.0 and the ratio increases with increase in $\frac{a}{h_1}$ ratio. So there is no significant difference between maximum normal stress ratio values for both homogeneous and nonhomogeneous interface either for soft layer on hard substrate $\frac{E_3}{E_1} > 1.0$ or for hard layer on soft substrate $\frac{E_3}{E_1} < 1.0$.

Again for normal stress as a function of distance curves for homogeneous and nonhomogeneous interface are overlapping each other as shown in Fig 8 , Fig 10, and Fig 12 So, we can conclude that for $0 < \frac{E_1}{E_3} < 13.33$ nonhomogeneous interface does not have significant effect on normal stress results.

4.4 Shear stress

Shear stress at the interface should be maintained below a critical value to prevent debonding between layer and substrate. We have obtained results for maximum shear stress at the layer-substrate interface σ_{xy} for both homogeneous and non homogenous interface for all the three types of indentors, for different Young's modulus ratio and for different $\frac{a}{h_1}$ ratio. Below are the values we have chosen for each parameter.

$$\frac{E_3}{E_1} : \frac{15}{200}, \frac{15}{120}, \frac{15}{60}, 1, \frac{60}{15}, \frac{120}{15}, \frac{200}{15}$$

$$\frac{a}{h_1} : \frac{1}{6}, \frac{1}{3}, \frac{1}{2}$$

Fig 14, Fig 16, and Fig 18 are plots showing how normalized interface shear stress, $\sigma_{xy}(\pi a^2)/L$ changes with distance from indentor axis along interface. Fig 15, Fig 17, and Fig 19 below are maximum shear stress ratio as a function of Young's modulus ratio plots for uniform indentor, flat indentor, and spherical indentor, respectively.

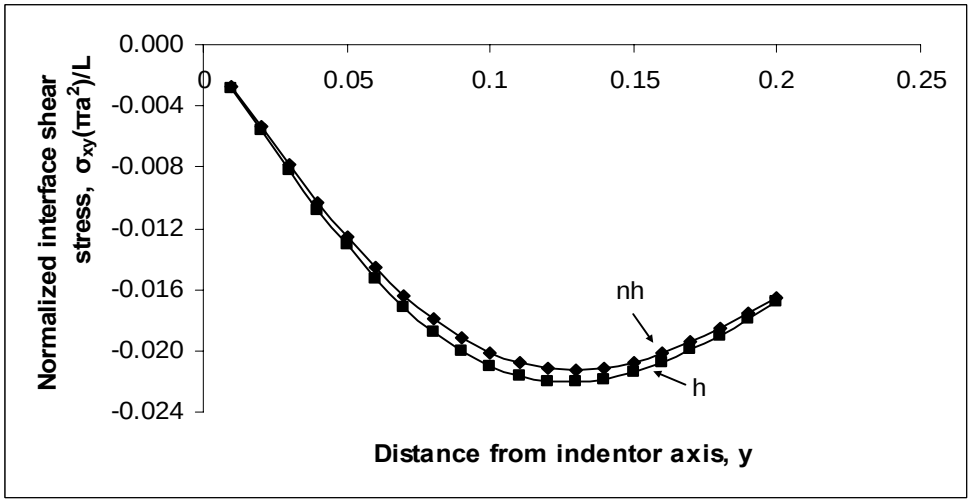

Figure 14: Normalized interface shear stress, $\sigma_{xy}(\pi a^2)/L$ at the layer-substrate interface as a function of distance along interface from indentor axis for uniform pressure

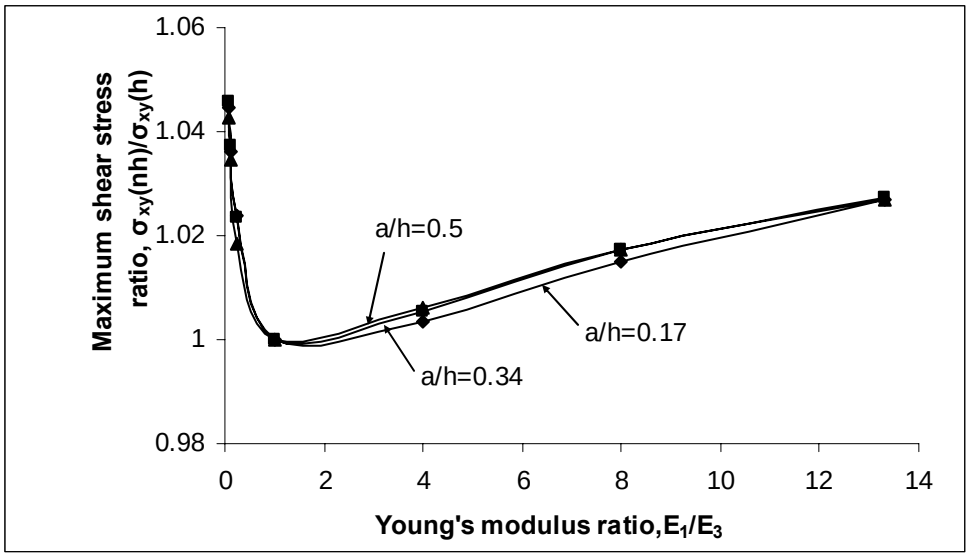

Figure 15: Maximum shear stress ratio along interface as a function of Young's modulus between layer and substrate for uniform pressure

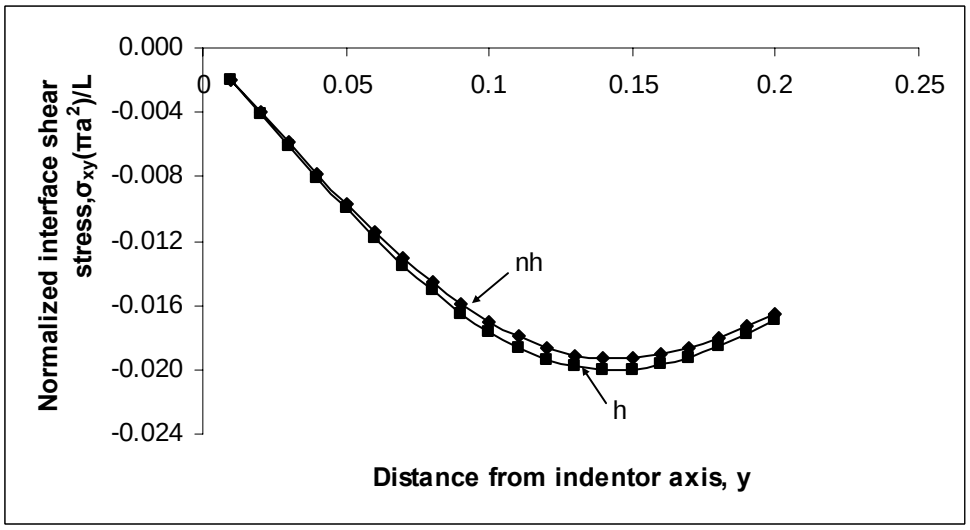

Figure 16: Normalized interface shear stress, $\sigma_{xy}(\pi a^2)/L$ at the layer-substrate interface as a function of distance along interface from indentor axis for flat indentor

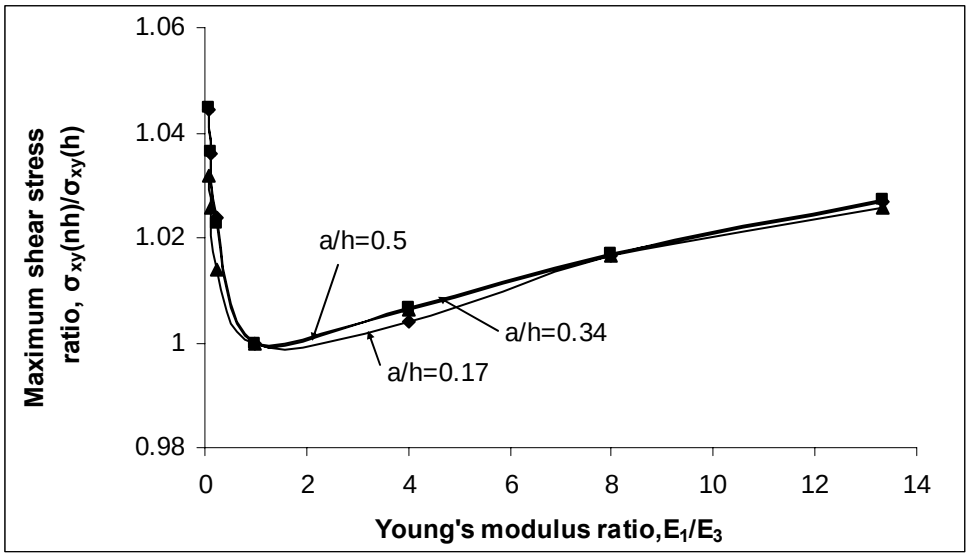

Figure 17: Maximum shear stress ratio along interface as a function of Young's modulus between layer and substrate for flat indentor

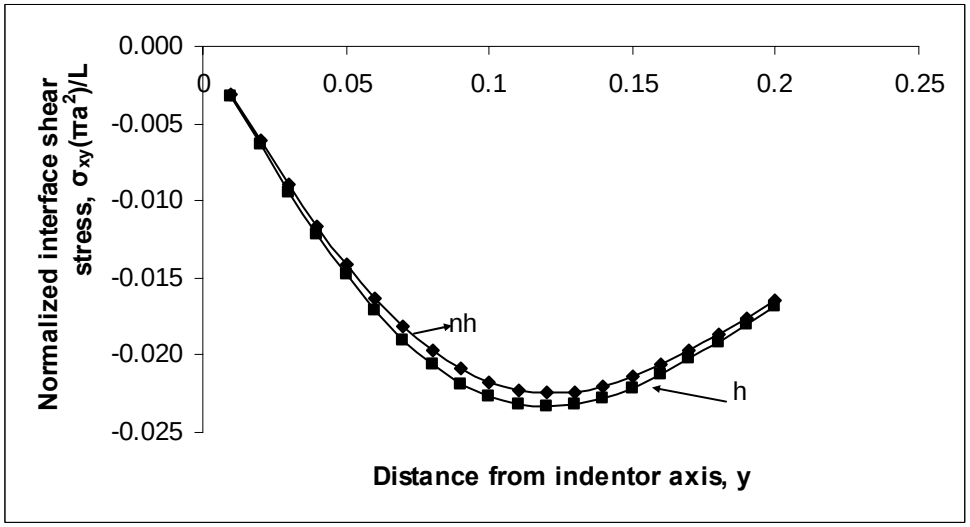

Figure 18: Normalized interface shear stress, $\sigma_{xx}(\pi a^2)/L$ at the layer-substrate interface as a function of distance along interface from indentor axis for spherical indentor

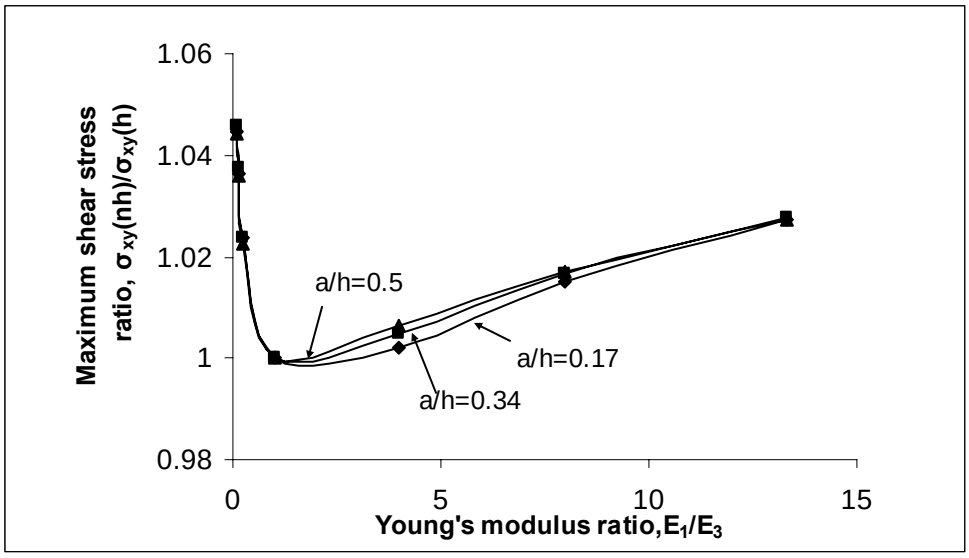

Figure 19: Maximum shear stress ratio along interface as a function of Young's modulus between layer and substrate for spherical indentor

We can see from the above plots the maximum shear stress ratio $\frac{\sigma_{xy}(nh)}{\sigma_{xy}(h)}$ is close to 1.0 and the ratio increases with increase in $\frac{a}{h_1}$ ratio. So there is no significant difference between maximum shear stress values for homogeneous and nonhomogeneous interfaces either for soft layer on hard substrate $\frac{E_3}{E_1} > 1.0$ or for hard layer on soft substrate $\frac{E_3}{E_1} < 1.0$.

We can also see from Fig 14, Fig 16, and Fig 18 that there is no significant difference between homogeneous and nonhomogeneous interface curves. So, we can conclude for $0 < \frac{E_1}{E_3} < 13.33$ nonhomogeneous interface does not effect shear stress results at the interface significantly.

4.5 Sensitivity analysis

The second part of study deals with using statistical analysis to quantify the effect of various factors on contact depth ratio, maximum normal stress ratio, and maximum stress ratio. For this purpose we have designed experiments using 2^4 factorial design discussed in previous chapter.

The four factors we have chosen for 2^4 factorial design in our study are

A) Type of indentor,

B) $\frac{h_2}{h_1}$ ratio,

C) $\frac{a}{h_1}$,

D) Young's modulus ratio $\frac{E_1}{E_3}$.

The above factors are chosen at two different levels. Table 3 shows the two levels chosen for each factor to execute 2^4 factorial design.

Table 3: Values of two different levels of the factors

Factor	Symbol	Level 1	Level 2
Type of indentor	A	Flat indentor	Spherical indentor
$\frac{h_2}{h_1}$	B	0.05	0.15
$\frac{a}{h_1}$	C	0.1667	0.5
$\frac{E_1}{E_3}$	D	$\frac{15}{200}$	$\frac{200}{15}$

4.6 Calculations

Using the above levels for factors as input we have calculated using the method described in previous chapter the percentage contribution of each factor by itself and together with other factors to a response.

Table 4, Table 5, and Table 6 below present percentage contribution of factors A-Type of indentor, B-ratio between interface width and layer width, C-ratio between indentor width and layer width, D-Young's modulus ratio and their combinations to contact depth ratio, maximum normal stress ratio, and maximum shear stress ratio respectively.

Table 4: Percentage contribution of factors to contact depth ratio

Factor	Effect Estimate	Sum of Squares	Percentage Contribution
A	-0.014160791	0.01203168	16.66
B	0.002276597	0.000310974	0.43
C	0.014212838	0.012120286	16.78
D	-0.013699431	0.011260465	15.59
AB	-0.002096113	0.000263621	0.36
AC	-0.013957742	0.011689113	16.18
AD	0.013795987	0.011419756	15.81
BC	-0.002096113	0.000263621	0.36
BD	-0.001850729	0.000205512	0.28
CD	-0.002096113	0.000263621	0.36
ABC	-0.001994151	0.000238598	0.33
ABD	0.001901632	0.000216972	0.30
ACD	0.01383597	0.011486044	15.90
BCD	-0.001890864	0.000214522	0.29
ABCD	0.00192271	0.000221809	0.30

Table 5: Percentage contribution of factors to maximum normal stress ratio

Factor	Effect Estimate	Sum of squares	Percentage Contribution
A	-0.0000823695	0.0000004071	0.39
B	-0.0006275050	0.0000236258	22.71
C	0.0002036027	0.0000024872	2.39
D	-0.0009689179	0.0000563281	54.15
AB	-0.0000458643	0.0000001262	0.12
AC	-0.0000606182	0.0000002205	0.21
AD	-0.0000648704	0.0000002525	0.24
BC	-0.0000458643	0.0000001262	0.12
BD	-0.0005713832	0.0000195887	18.83
CD	-0.0000458643	0.0000001262	0.12
ABC	-0.0000345889	0.0000000718	0.069
ABD	-0.0000341496	0.0000000700	0.067
ACD	-0.0000477291	0.0000001367	0.13
BCD	0.0000830774	0.0000004141	0.39
ABCD	-0.0000260699	0.0000000408	0.039

Table 6: Percentage contribution of factors to maximum shear stress ratio

Factor	Effect Estimate	Sum of squares	Percentage Contribution
A	0.00002778	0.0000000463	0.021
B	-0.0013148942	0.0001037368	47.06
C	-0.0000566192	0.0000001923	0.087
D	0.0010163401	0.0000619768	28.11
AB	0.0000916392	0.0000005039	0.22
AC	0.0000441751	0.0000001171	0.053
AD	-0.0000467626	0.0000001312	0.059
BC	0.0000916392	0.0000005039	0.22
BD	0.0008835317	0.0000468377	21.24

Table 6: Continued

CD	0.0000916392	0.0000005039	0.22
ABC	0.0000751591	0.0000003389	0.15
ABD	-0.0000674468	0.0000002729	0.12
ACD	-0.0000233928	0.0000000328	0.014
BCD	-0.0002831228	0.0000048095	2.18
ABCD	-0.0000827806	0.0000004112	0.18

From Table 5 we can see that the contribution of individual factors A (Type of load), C (Indentor width to layer width ratio,a/h_1) and D (Young's modulus ratio E_3/E_1) to contact depth ratio response is significant and almost equal (close to 15%) where as contribution from B (Interface width to layer width ratio, h_2/h_1) is minimum(0.43%). So, we can conclude that contact depth ratio response equally depends on A (Type of indentor), C (Indentor width to layer width ratio, a/h_1), D (Young's modulus ratio, E_3/E_1) and the influence of B (Interface width to layer width ratio, h_2/h_1) on contact depth ratio is minimum.

From Table 6 we can see that maximum normal stress ratio response has largest contribution from D-54.15% (Young's modulus ratio, E_3/E_1) followed by B-22.71% (Interface width to layer width ratio, h_2/h_1).The contributions of A (Type of load) and C (Indentor width to layer width ratio, a/h_1) are 0.39% and 2.39%, respectively. So, we can conclude that D (Young's modulus ratio, E_3/E_1) is the most significant factor and A (Type of load) is the least significant factor for maximum normal stress ratio.

From Table 7 we can see that B (Interface width to layer width ratio, h_2/h_1) followed by D (Young's modulus ratio, E_3/E_1) with contributions 47.06% and 28.11%,

respectively are significant factors for maximum shear stress response and contributions from A (Type of load) and C (Indentor width to layer width ratio, a/h_1) are 0.027% and 0.087%, respectively. So, we can conclude that B (Interface width to layer width ratio, h_2/h_1) is the most significant factor and A (Type of load) is the least significant factor for normal shear stress response.

CHAPTER 5

CONCLUSIONS

The objective of this study is to study the effect of various parameters involved in layer-substrate indentation experiments on final results. We have shown that either for soft layer on hard substrate or for hard layer on soft substrate the results for contact depth, maximum normal stress and maximum shear stress are almost same for homogeneous change of Young's modulus at the interface and nonhomogeneous change of Young's modulus at the interface. So, we cannot conclude whether the interface is homogeneous or nonhomogeneous using contact depth results from layer-substrate indentation experiments for Young's modulus ratio less than $13.33\left(\frac{E_1}{E_3} < 13.33\right)$.

Also, using statistical analysis we have quantitatively found the effect of various factors on contact depth ratio, maximum normal stress ratio and maximum shear stress ratio. Young's modulus ratio followed by ratio between interface thickness and layer thickness have major impact on both maximum normal stress ratio and maximum normal stress ratio where as the impact of type of load and indentor width- layer thickness ratio is insignificant. Also, Young's modulus ratio, indentor width-layer thickness ratio and type of load have equal and significant impact on contact depth ratio where as ratio between interface thickness and layer thickness has no significant impact on contact depth ratio.

Although, conclusions on the effect of nonhomogeneous interface are based on restricted choice of Young's modulus ratio, our study is a good start in characterization of interface which is important in design and deposition of thin films on substrates. In the next part of our study we propose to overcome the limitations on Young's modulus ratio by modeling the interface as multiple nonhomogeneous thin sub strips with Young's modulus and Poisson's ratio varying exponentially across each sub strip thickness.

Further, sensitivity analysis provides valuable information about the impact of various parameters on indentation results which can be used in design and mechanical characterization of layer-substrate combinations.

REFERENCES

Chudoba, T., Schwarzer, N. and Richter, F. *Determination of elastic properties of thin films by indentation measurements with a spherical indenter.* Surface and Coatings Technology 127 (2000), P. 9-17.

Chudoba, T., Schwarzer, N., Linss, V., Ritcher, F. *Determination of mechanical properties of graded coatings using nanoindentation.* Thin Solid Films 469-470 (2004), P. 239-247.

Delale, F. and Erdogan, F. *On the mechanical modeling of the interfacial region in bonded half-planes*. ASME Journal of Applied Mechanics 55 (1988), P. 317-324.

Doerner, M.F. and Nix, W.D. *A method for interpreting the data from depth sensing indentation instruments.* Journal of Materials Research 1 (1986), P. 601-609.

Gupta, G.D. *A layered composite with a broken laminate.* International Journal of Solids and Structures 9 (1973) 1141-1154.

Kaw, A.K., Selvarathinam, A.S. and Besterfield, G.H. *Comparison of interphase models in a fracture problem in fiber reinforced composites*. Journal of Theoretical and Applied Mechanics 17 (1992), P. 133-147.

Linss, V., Schwarzer, N., Chudoba, T., Karniychuk, M., Richter F. (2004). *Mechanical properties of a graded B-C-N sputtered coating with varying Young's modulus: deposition, theoretical modeling and nanoindentation.* Surface and Coatings Technology 195 (2005), P. 287-297.

Montgomery, D.C. 2001, *Design and analysis of experiments,* John Wiley & Sons, Inc. New York.

Oliver, W.C., Hutchings, R., and Pethica, J.B. *Microindentation Techniques in materials science and engineering*. ASTM STP 889, edited by P.J. Blau and B.R. Lawn. American Society for Testing and Materials (1986), P. 90-108.

Oliver, W.C and Pharr G.M. *An improved technique for determining hardness and elastic modulus using load and displacement sensing indentation experiments.* Journal Materials Research 7 (1992), P. 1564-1583.

Shaohua, Lei, Tzuchiang. *Investigation of mechanical properties of thin films by nanoindentation, considering the effects of thickness and different coating-substrate combinations.* Surface and Coatings Technology. 191 (2005), P. 25-32.